Environ Earth Sci (2011) 64:539–547
DOI 10.1007/s12665-010-0877-8

ORIGINAL ARTICLE

Chemistry of the Ferraria thermal water, S. Miguel Island, Azores: mixing and precipitation processes

Maria do Rosário Carvalho · António Mateus · João C. Nunes · José M. Carvalho

Received: 30 April 2010 / Accepted: 16 November 2010 / Published online: 5 December 2010

Abstract The Ferraria thermal water emerges at the sea level in the Ferraria lava delta (western edge of S. Miguel Island, Azores) with temperature of ca. 60°C and pH varying between 5.4 and 6.2. It is of sodium chloride type, resulting from ca. 50% seawater mixing with an acid brackish, at ≈100°C, denoting the presence of significant CO_2(g) and the progress of water–rock interactions in open system conditions. The thermal Na–Cl water is strongly enriched with Sr and Mn and, comparatively, has low concentrations in Al, Fe and As. These elements are removed from the solution as critical conditions for the formation of several neo-formed mineral phases are gradually attained. Thermodynamic equilibrium calculations are consistent with this interpretation, showing that the thermal fluid can precipitate Fe^{3+}-(hydr-)oxides, kaolinite and non-crystalline silica. Wells logging show fracture planes and pores fully/partly filled up with polyphase botryoidal aggregates mostly composed of goethite + ferrihydrite and displaying variable adsorbed contents of Si, P and As. These neo-formed phases result from the pristine fluid oxidation due to seawater mixing; its precipitation is easily affected by pH and redox variations of the brackish, due to volcanic gases pressure alterations, and fluid pressure or flow-velocity oscillation in the fractured aquifer.

Keywords Thermal water · Hydrochemistry · New-formed phases · S. Miguel Island (Azores)

M. R. Carvalho (✉) · A. Mateus
Departamento Geologia and CeGUL, Faculdade de Ciências, Universidade de Lisboa, Ed.C6, Campo Grande, 1749-016 Lisbon, Portugal
e-mail: mdrcarvalho@fc.ul.pt

A. Mateus
e-mail: amateus@fc.ul.pt

J. C. Nunes
Departamento Geociências, Universidade dos Açores and INOVA, Instituto de Inovação Tecnológica dos Açores, Estrada de São Gonçalo, 9504-540 Ponta Delgada, Açores, Portugal
e-mail: jcnunes@uac.pt

J. M. Carvalho
Dep. Eng. Geotécnica, Instituto Superior de Engenharia do Porto, R. Dr. Bernardino Ribeiro, 431, 4200-072 Porto, Portugal
e-mail: jmc@tarh.pt

Introduction

The Ferraria thermal water emerges at the sea level with a temperature of *ca.* 60°C in the western edge of the S. Miguel Island (Ponta da Ferraria), having supplied the nearby thermal hospital during its running (1880–1970). The water spring is hosted in the Ferraria lava delta, part of the Sete Cidades Volcano (Fig. 1) to which other chemically similar thermal springs are related; the latter show lower temperatures (30–43°C) and are mostly located at the Mosteiros graben, whose geothermal resources have an energetic potential of ca. 8 MWe (Forjaz 1994).

In order to evaluate the possibility of reactivating the Ferraria thermal facility, a set of studies were scheduled and carried out by the Azores Government and the INOVA Institute on three wells (AC1, AC2 and AC3; Fig. 1) which prove to have water with suitable temperature and enough flow-rate for that purpose. The AC3 monitoring reveals that the thermal water chemical features are within the required standards, but not all the element concentration fluctuations in time are explained on the basis of variations in [seawater]:[thermal fluid] mixing proportions, occasionally attaining levels that need a proper explanation. This

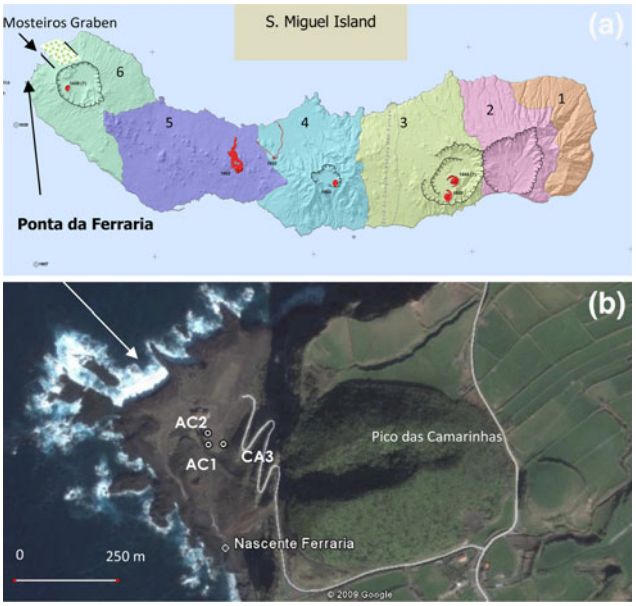

Fig. 1 **a** Volcanic complexes of S. Miguel Island, Azores (*1* Nordeste, *2* Povoação, *3* Furnas, *4* Fogo, *5* Picos, *6* Sete Cidades) and Ponta da Ferraria lava delta location; **b** location of AC1, AC2 and AC3 wells, besides the thermal spring ("Nascente Ferraria"). Adapted from Nunes (2004)

problem will be addressed in the present work, making use of a multi-disciplinary approach that combines a full chemical characterisation of the thermal waters pumped in AC3 and a comprehensive examination of the hosting rocks in order to investigate the reasons for that composition fluctuation with time.

Geological synopsis

The Sete Cidades Volcano is one of the four silicic polygenic volcanoes with caldera in S. Miguel Island. It is a stratovolcano with an inferred age of 800 Ka, rising up to 2,700 m above the surrounding seafloor that displays a base diameter of $\approx$14 km and covers an area of $\approx$122 km^2; the summit caldera has an average diameter of 5.3 km and a maximum depth of 620 m (Nunes et al. 2004). Its eruptive history is recorded by basaltic s.l. (sensu lato) lava flows and pyroclasts, trachytic s.l. lava flows, domes and pumice fall deposits, and ignimbrites, surges and lahar deposits.

The Ponta da Ferraria is a basaltic s.s. (sensu stricto) lava delta, with a triangular shape and finger-like shoreline contour, covering an area of $\approx$0.1 km^2 (Fig. 1). The aa-type lava flow that makes this delta extruded from the Pico das Camarinhas (one of the 46 flank eruptions of the Sete Cidades Volcano; Nunes et al. 2004) during a strombolian-type volcanic eruption dated to 840 $\pm$ 60 years B.P. (Moore 1991); information gathered from AC1 and AC2 drill-holes reveals that this lava flow has an average thickness of $\approx$22 m, including the top and bottom clinker layers.

Besides the regional base aquifer, the main hydrogeological features of the Sete Cidades Volcano consist of perched aquifers recharged by meteoric water through the volcanic caldera (lakes) and slopes (Coutinho 1990).

Sampling and analytical methods

The Ferraria thermal water was sampled in April and October 2008 at the AC3 well, after some minutes of continuous pumping. The temperature, pH, conductivity, redox potential and H_2S were measured in situ. The H_2S determination involved titration with mercuric acetate using dithizone for the end-point detection with a lower limit of 0.01 ppm (Arnórsson 1991). Samples for cation analysis were filtered with a 0.45 μm filter pore-diameter, acidified with ultra-pure nitric acid and further analysed by AAS, ICP-MS and ICP-OES. Samples for anion analysis were kept un-acidified and subsequently analysed by potentiometry and ion chromatography. Samples for silica analysis were acidified and diluted with distilled water in a proportion of 1:2 to prevent polymerisation. In order to determine the total dissolved inorganic C, avoiding its escape as CO_2, 250 mL of water was also collected adding 1 mL of a NaOH solution 5 N. The free CO_2, alkalinity, total dissolved H_2S and silica determinations were made at the INOVA-certified laboratory facilities. Ion chromatography analyses were carried out at FCUL and those involving ICP-MS and ICP-OES methods at the Activation Laboratories Ltd. Additional δ^2H, δ^{18}O and δ^{13}C measurements were performed by mass spectrometry (SIRA 10–VG ISOGAS) at the Instituto Tecnológico e Nuclear (ITN, Portugal). The δ^{13}C water samples were filtered precipitates obtained through the addition of 100 g of BaCl immediately after the sampling of 1 L of thermal water in a polyethylene bottle, previously prepared with 5 mL of a NaOH solution 5 N. The δ^{34}S determination was performed at the Activation Laboratories Ltd. in water samples without any specific treatment.

During the April survey, the cores of AC1 and AC2 drill-holes were examined and five representative samples of each drilled section were picked for subsequent petrographical and geochemical studies. The whole-rock analyses were performed in the Activation Laboratories Ltd., according to the combined analytical package 4E-Research, 4E-ICP/MS, 4F for S and 4F for Hg; details on the analytical methods used, as well as the respective detection limits, can be checked in http://www.actlabs.com/gg_rock_litho_usa.htm.

Table 1 Representative physical–chemical analyses of the Ferraria thermal water pumped at AC3 well

Parameter	AC3		
Date	11/Abr/08		15/Out/08
Tide	Low-tide	High-tide	High-tide
Temperature (°C)	60.7	60.6	61
pH at 20°C	5.45	5.41	6.16
Eh (mV)	134	100	
Conductivity (mS/cm)	36.9	36.9	32.6
Alcalinity	570	569	
Free CO_2	351	86	
H_2S (mg/L)	0.06	0.04	0.02
NO_3 (mg/L)	<2.6		
NH_4 (mg/L)	0.03		
SiO_2 (mg/L)	168	130	189
HCO_3 (mg/L)	695.4	694.2	
SO_4 (mg/L)	1,050	1,078	1,388
F (mg/L)	0.7		
Cl (mg/L)	9,650	9,560	9,848
Li (mg/L)	0.63	0.62	0.6
Na (mg/L)	5,600	5,500	5,370
K (mg/L)	221	332	232
Mg (mg/L)	529	185	349
Ca (mg/L)	294	268	200
Sr (μg/L)	6,300	6,100	5,950
Ba (μg/L)	10	17	50
Mo (μg/L)	35	35	40
Mn (μg/L)	1,940	490	1,410
Fe (μg/L)	460	770	530
Co (μg/L)	<6	<6	3.7
Ni (μg/L)	32	14	<30
Cu (μg/L)	<0.05	<0.05	<20
Zn (μg/L)	40	50	120
Cd (μg/L)	1.1	1.1	<1
B (μg/L)	4,500	3,300	4,200
Al (μg/L)	230	49	<200
Pb (μg/L)	19	16	6
As (μg/L)	166	329	212

Results

Water chemistry

Table 1 displays representative data for the thermal fluid sampled at AC3 well. The water temperature is of the order of 60°C; the maximum value measured was 61.8°C. In April, the water pH slightly decreased along the pumping time-span, reaching 5.45 and 5.41 in low and high tide conditions, respectively; in October, the pH was 6.16. The electrical conductivity, although quite low at the pumping onset, quickly stabilised around 37 and 32.6 mS/cm in April and October, respectively. The total dissolved H_2S is rather low, being close to the detection limit of the used method (i.e. 0.01 ppm).

A simple inspection of the analytical data shows that the electrical conductivity values reflect totals of dissolved species around ½ of the seawater average mineralisation. The pH, resting below the one that characterises seawater (pH 8), strongly suggests that the mixed thermal fluid is significantly more acidic ($pH < 5$).

The thermal water is of sodium chloride type, as the result of seawater mixing. Its composition denotes also water–rock interactions in open system conditions besides significant CO_2(g). Therefore, the relative depletion in sulphate and magnesium is interpreted as a result of their incorporation in neo-formed mineral phases (such as Mg-bearing phyllosilicates and Fe^{3+}-Al-bearing sulphates). Normalising the thermal water composition in relation to seawater provides evidence for (1) extensive dilution of the major marine species (Na, Cl, SO_4, Mg) contents; (2) lesser dilution of Ca contents; (3) considerable enrichment in CO_2, SiO_2, Li, Mo, Mn, Al and As; and (4) noteworthy depletion of Zn and Cd contents. The thermal water chemical monitoring performed by INOVA during the time span between February and September 2008 shows, additionally, that (1) CO_2(g) varied from 190 to 580 mg/L (with minimum values in March and June), although without influencing notably the alkalinity; (2) SO_4, Na and Mg contents increased from April to July (peaking 1,130, 6,070 and 615 mg/L in March), which seems to reflect a larger proportion of seawater in the mixture; (3) chloride contents co-varied with SO_4 and Na, excepting the sample collected in March; and (4) K contents fluctuated largely, not following the variation pattern of any dissolved main species.

During the monitoring period, anomalously high As and Fe contents (329 and 770 μg/L, respectively) were detected in April in the water sampled at high-tide conditions (Table 1). It should be noted that, for logistical reasons, the analysis was performed several days after the water sampling. However, given the tendency usually revealed by As to be adsorbed by the colloidal or Fe^{3+}-hydroxide phases meanwhile precipitated, the As content increasing cannot be satisfactory explained by that hiatus. Alternatively and because the sample subjected to analysis was not filtered in situ, it is suggested that those high values reflect the presence of solids in suspension transferred to the pumped water due to particular conditions created during the multiple well pumping operation, i.e. sudden shutting of the discharge triggered in the morning period, at low-tide conditions, followed by well reopening in the course of the high-tide time; this should have caused a pressure raise of the thermal fluid retained within rock fractures/pores,

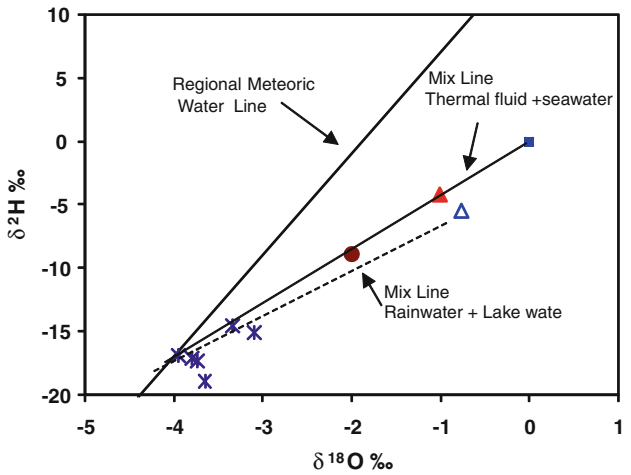

Fig. 2 δ^2H and δ^{18}O ($^o/_{oo}$ vs. V-SMOW) isotopic compositions for the Ferraria thermal water (*red triangle*; INOGAZ project); cold water springs (*blue star*) and lake water (*triangle*), (Coutinho et al. 1996); seawater (*blue square*); pristine fluid (*brown circle*)

enough to raze Fe^{3+}-(hydr)oxide precipitates with adsorbed As therein previously formed, thus removing these components to the water flow. It should be noted that the As content showed by the thermal water collected in October under high-tide conditions exceeded the value reported for April (at low-tide conditions), possibly reflecting the effects of a higher fluid pH, which allows keeping As in solution.

The δ^2H and δ^{18}O isotopic composition of the Ferraria thermal water is −4.17 and −1.0‰, respectively. Considering the available data together with δ^2H and δ^{18}O values of seawater and regional meteoric waters (Carvalho 1999), one may infer that the analysed thermal water is a result of seawater mixing with a (pristine) fluid characterised by −18‰ δ^2H and −3.8‰ δ^{18}O values (Fig. 2). This composition is compatible with the isotopic range reported by Coutinho (1990) and Coutinho et al. (1996) for water springs and cold-water wells located in the Sete Cidades Volcano, between 60 and 750 m of altitude (i.e. [−22, −15]‰ δ^2H and [−4.3, −3.1]‰ δ^{18}O); the spring at the lowest altitude is, indeed, fed by a fluid with isotopic features quite close to those inferred for the non-seawater component at Ferraria, i.e. −20.7‰ δ^2H and −4.03‰ δ^{18}O. The δ^{13}C value obtained for the dissolved C in the Ferraria thermal water (−3.83‰) denotes a CO_2 mantle source and is similar to other isotopic determinations in fumaroles and thermal springs related to the Furnas and Fogo volcanogenic systems (Carvalho 1999; Cruz et al. 1999). The δ^{34}S value (20.25‰) of the Ferraria thermal water reflects, as expected, a marine S source; indeed, even in presence of a distinct ^{34}S source, the large predominance of seawater in the mixture obliterates its tracing.

Thermal wells' logging, mineralogy and geochemistry

AC1 drill-hole

The AC1 drill-hole reached the depth of 25.5 m. Macroscopic inspection of the cores allows concluding that (Fig. 3a) (1) there is no evidence for thermal fluid circulation in the vesicular basalts until ≈10.80 m depth; (2) from that depth till 13.20 m, some of the fractures that cross the compact basalt (with abundant xenoliths) show effects caused by thermal fluid flow: these effects are limited to heterogeneous discoloured halos adjoining fracture planes, which rarely extend over than 1 cm; (3) from 13.20 m to 21.35 m depth, the record of fracture-controlled hydrothermal circulation in compact basalt (with lesser xenoliths and low vesicle content) is increasingly stronger: fractures tend to develop a reasonable inter-connected network, rather significant between 18 and 19 m of depth, suggesting the possibility of this basaltic level corresponding to the "outer domain" of fluid escaping, particularly during events of system depressurising; (4) from 21.35 to 24.4 m depth, the volcanic rock (massive, with low vesicle content from 22.7 to 24.4 m) preserves features due to (pervasive) interaction

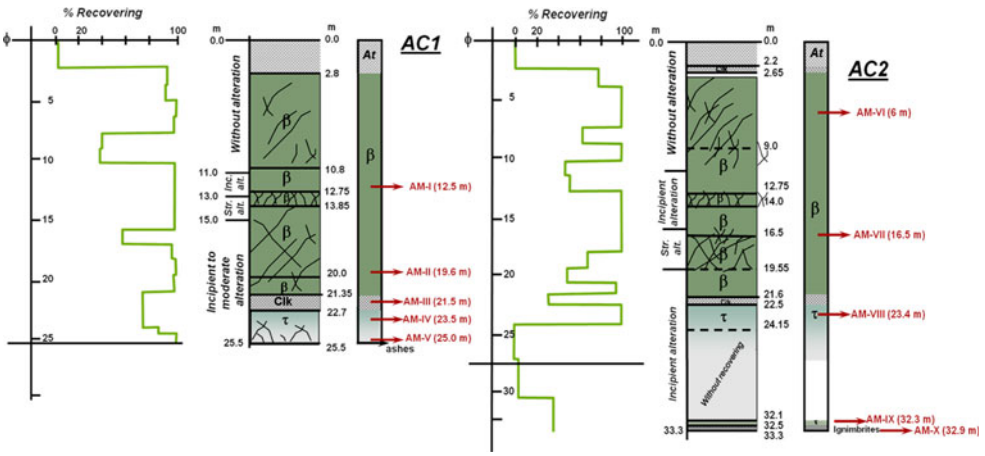

Fig. 3 Schematic *logs* for AC1 (**a**) and AC2 (**b**) drill-holes and samples positioning

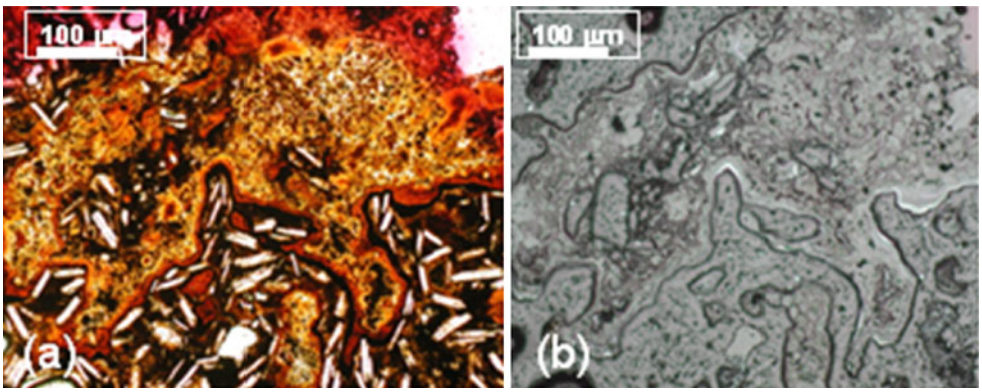

Fig. 4 Photo-micrographs illustrating the late Fe^{3+}-bearing precipitates in AM-V sample (AC1 drill-hole). Transmitted, simply polarised light for image **a**; reflected, simply polarised light for **b** image, revealing that only some of the late bands are made of goethite (*light-grey* phase with higher reflectance)

with thermal fluids, comprising neo-formed mineral assemblages that include phases belonging to the zeolite and sulphate groups, besides finer disseminations (micro-fissuring controlled) of partly oxidised pyrite and scarce chlorite/smectite; (5) from $\approx$24 to 25.5 m of depth, the (oxidising) alteration is quite strong, leading to abundant Fe (hydr-) oxides and jarosite.

Comprehensive petrography of selected samples (AM-I to AM-V; see Fig. 3a for sampling depths) shows that basalts represented by AM-I and AM-II have a noteworthy micro-porosity heterogeneously distributed. In these rocks, feldspar s.l. microliths form a well-developed network whose interstitial spaces are filled with irregular pyroxene grains (usually optically zoned), olivine (not always preserved), magnetite (micro-millimetric grains, locally abundant and sometimes displaying ilmenite lamellae) and rare amphibole; feldspar and pyroxene (micro-)phenocrysts occur occasionally. With the exception of sporadic optical effects reflecting incipient (and local) magnetite oxidation and peripheral feldspar corrosion, there are no other evidence ascribable to mineral-textural transformations triggered by hydrothermal alteration. In AM-II, a xenolith made of poikilitic feldspar grains surrounded by a fine-grained amphibole aggregate can be observed; in AM-I, late pyrite and chalcopyrite are also present in the rock matrix, forming micrometric and irregular grains heterogeneously distributed.

The basaltic rock represented by AM-III is similar to the one typified by AM-I and AM-II, regardless of the higher (and macro-)porosity; its matrix granularity is finer, the amphibole microliths more common and the feldspar and pyroxene micro-phenocrysts more abundant, the larger grains showing often reaction rims. In this basaltic level, magnetite occurs as millimetre rounded grains, free of ilmenite lamellae or of features due to late oxidation and coexist with many other (sub-)micrometric grains that, only sporadically, reveal sub-idiomorphic morphology; evidence of silicate significant hydrothermal alteration is also missing; there are, however, scarce (sub-)micrometric grains of pyrite near to magnetite, the larger one displaying a peripheral hale of magnetitic composition.

The mineralogical nature of AM-IV supports its classification as trachybasalt, presenting a relatively coarse matrix mostly composed of plagioclase and feldspar and including as accessory phases amphibole (with bimodal granularity), magnetite, biotite and pyroxene. Magnetite grains are predominantly sub-micrometric and sub-idiomorphic, locally displaying skeletal morphologies denouncing rapid cooling; often, these spinels record effects of significant oxidation, as reflected by hematite rimming and intra-granular infillings. Larger plagioclase grains show also evidence of local and incipient hydrolysis, which leads to formation of secondary assemblages comprising fine-grained muscovite and quartz.

The AM-V sample mineralogy (25 m depth) is quite different from those afore-mentioned; it represents a porous layer strongly altered by means of hydrolysis and oxidation processes, which lead to the almost complete destruction of primary Fe/Mg-bearing silicates and feldspars s.l. Consequently, the corroded feldspar microliths emerge from a groundmass quite enriched with poorly crystallised Fe-hydroxides wherein is still possible to identify relics of deeply oxidised spinels (maghemite-hematite), (Fig. 4). The macro- and micro-pores are fully or partly filled up with polyphase botryoidal aggregates that locally show rhythmic growing and are mostly composed of goethite and other Fe-rich phases, as further confirmed by electron microprobe studies (Fig. 5). The latter investigations show also the many of these late growing bands are enriched with Si, P and, locally, As, thus suggesting the presence of poorly crystallised ferrihydrite with variable adsorbed contents in those elements.

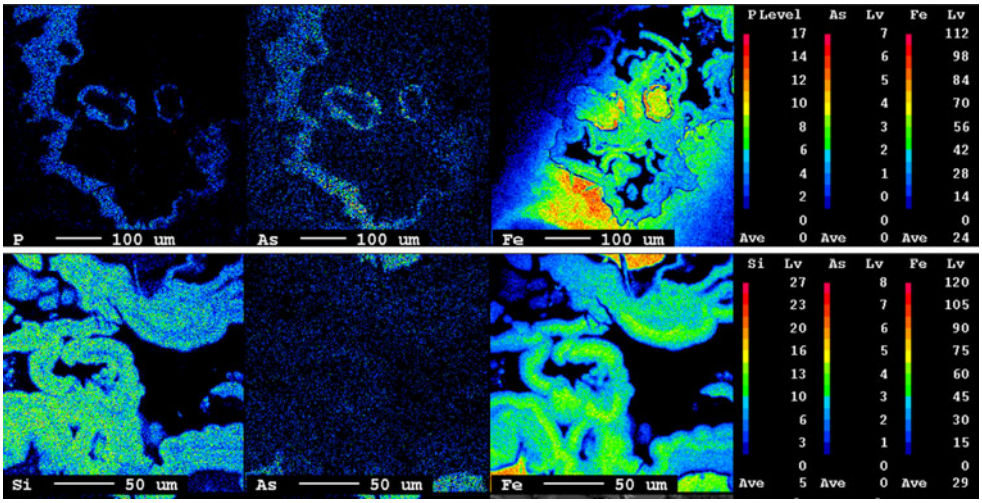

Fig. 5 Chemical composition maps of two representative domains of the late Fe^{3+}-bearing precipitates in AM-V (AC1 drill-hole) obtained with the JEOL-JXA electron microprobe

The whole-rock geochemistry data obtained for AC1 samples (Table 2) are compatible with their mineralogical features, the relatively anomalous contents of S and Cu (±As) revealed by AM-I (4,900, 3,820 and 15 ppm, respectively), and the high As content displayed by AM-V (574 ppm) being worth noting. The fairly consistent concentrations of Co (30–40 ppm, excepting AM-IV), Cu (scattered between 130 and 376 ppm) and Zn (ranging from 75 and 130 ppm) are also significant.

AC2 drill-hole

The AC2 drill-hole reached the depth of 33.3 m. As in AC1, five samples were picked from AC2 cores for petrography and geochemical studies, representing the most critical features observed macroscopically (see Fig. 3b for log and sampling depths). The AM-VI specimen characterises a basaltic rock with macro-porosity and clear evidence of alteration, showing pyroxene and feldspar (micro-)phenocrysts, besides matrix-interstitial olivine, amphibole and magnetite; olivine (micro-)phenocrysts only occur occasionally and, when that happens, they are surrounded by a very fine-grained aggregate of pyroxene and Ti-rich magnetite. Magnetite is relatively abundant, and the larger grains (sporadically displaying fine ilmenite lamellae) tend to form clusters of millimetric dimension. The observed micro-xenoliths are composed of plagioclase, pyroxene and spinel (Ti-magnetite and/or ulvospinel).

Sample AM-VII differs from AM-VI in some distinctive features. Magnetite is quite common and forms two granulometric classes, the micrometric one prevailing and including sub-idiomorphic grains that, locally, coexist with rare pyrite. The coarser oxide class comprises titanomagnetite grains with ilmenite lamellae, besides mix-magnetite/ilmenite grains that tend to occur preferentially within xenoliths or along their borders; rare magnetite grains preserve fine (drop-type) pyrite inclusions. The silicate assemblage is the usual in this kind of rock (plagioclase, pyroxene, olivine, and amphibole) the former two mineral phases displaying often reaction rims. The (micro-) phenocrysts are exclusively of plagioclase, which prevails also in xenoliths where they are enclosed in a fine matrix quite rich in pyroxene and (Ti-)magnetite. In xenoliths, the inter- and transgranular fracturing is particularly intense (as a result of the rheological contrast with the basaltic envelop), allowing the late development of Fe^{3+}-bearing precipitates optically similar to those reported for AM-V, besides the sporadic interstitial growth of calcite and anhydrite (or gypsum?); it should be noted that the Fe^{3+}-bearing precipitate formation postdates the deposition of carbonate (±sulphate).

The AM-VIII and AM-IX samples represent a trachytic rock with significant micro-porosity and comprising abundant feldspar and plagioclase micro-phenocrysts supported by feldspar/amphibole-rich matrix with rare pyroxene. The latter two silicates show corrosion/alteration rims, quite rich in oxides ± chlorite. Primary oxides (mainly magnetite) display evidence of moderate to strong oxidation, regularly following the spinel octahedral partition planes and quite obvious in coarser grains. Feldspar display commonly late zoned growth but effects recording their hydrolysis are rather exceptional.

The AM-X sample corresponds to an ignimbrite incorporating heterometric fragments of variably oxidised trachyte; the groundmass displays significant porosity and is composed of a fine-grained siliciclastic aggregate wherein occur scarce phenocrysts fragments of diverse nature (plagioclase, pyroxene and amphibole); some of the pores are filled by late zeolitic masses. The oxides are present in two different textural settings: within trachytic fragments and in transitional fragment/matrix strips; in any circumstances, the (Ti-)magnetite prevails.

Table 2 Whole-rock analyses of representative samples from the cores of AC1 and AC2 drill-holes

Sample code	SiO_2 %	Al_2O_3 %	Fe_2O_3(T) %	MnO %	MgO %	CaO %	Na_2O %	K_2O %	TiO_2 %	P_2O_5 %	Mo ppm	As ppm	Co ppm	Cr ppm	Cd ppm	Cu ppm	Ni ppm	Zn ppm	S %
AMI-AC1	46.29	15.26	12.75	0.195	6.43	10.1	2.98	1.72	3.497	0.86	6	15	41.8	171	1.2	3,820	57	129	0.141
AMII-AC1	46.54	16.03	11.22	0.19	5.33	10.25	3.42	1.86	3.463	0.82	4	4	42.1	157	1.1	376	57	108	0.051
AMIII-AC1	46.42	15.37	12.03	0.177	5.85	10.29	3.2	1.82	3.637	0.8	5	5	42.2	191	1	221	59	95	0.049
AMIV-AC1	58.3	17.96	5.52	0.167	1.23	3.21	5.72	4.4	1.281	0.31	4	9	4.3	<0.5	<0.5	213	5	118	0.04
AMV-AC1	52.85	14.34	12.96	0.703	0.88	2.2	4.78	3.71	1.039	0.54	18	392	34.1	19.3	1.1	132	13	76	0.086
AMVI-AC2	46.77	15.43	11.91	0.193	6.26	9.65	3.32	1.72	3.363	0.8	3	4	44.3	164	1	122	58	103	0.027
AMVII-AC2	45.02	15.42	13.07	0.205	6.37	10.52	3.17	1.61	3.629	1.09	4	9	40.3	151	1.1	114	50	112	0.018
AMVIII-AC2	58.11	17.52	5.37	0.142	1.2	3.1	5.62	4.32	1.252	0.31	4	17	4.7	14.4	0.6	147	5	144	0.052
AMIX-AC2	58.28	17.99	5.52	0.154	1.2	3.25	5.7	4.32	1.279	0.31	4	8	4.7	<0.5	<0.5	89	5	111	0.024
AMX-AC2	55.33	16.72	5.26	0.137	1.19	2.26	4.43	3.68	0.98	0.2	6	8	9.5	65.1	<0.5	50	23	103	0.028

In what concerns the geochemical features (Table 2), it should be emphasised the higher content in As (17 ppm) and S (1,400 ppm) showed by AM-VII, relatively to the remaining four samples, which is compatible with the above-referred mineralogical characteristics. The existing contrast between the Cu, Ni and Co contents in AM-VI and AM-VII (115–150 ppm, 50–60 ppm and 40–44 ppm, respectively) in relation to those displayed by the other samples analysed (<90, <20 and <10 ppm, respectively) is, as well, noteworthy.

Discussion and conclusions

The data here reported for water pumped in AC3 well is consistent with published information concerning the AC2 well and Ferraria thermal spring (Freire 2006), denoting variable degrees of seawater mixing with a pristine volcanic fluid. A similar pattern is recognised for the thermal water of Mosteiros, which emerges at 30–43°C, shows lower mineralisation and records equivalent concentrations of dissolved CO_2(g).

Due to its mineralisation ($\approx$½ of seawater), the Ferraria thermal water is not simply seawater heated by the local high geothermal gradient. Indeed, taking into account the temperature, electric conductivity and Na/Cl ratio displayed by the AC3 water and seawater, one may conclude that the Ferraria thermal water has similar composition to seawater diluted by 50%; in comparison to seawater, it is depleted in sulphate and magnesium (as a result of precipitation), and relatively enriched with calcium (possibly due to basaltic rocks dissolution). The thermal fluid mixed with seawater corresponds to an acid brackish at $\approx$ 100°C, enriched with volcanic gases [namely CO_2(g)] and able to react chemically with hosting rocks. Therefore, significant dissolution of reactive volcanic gases sustains the hot acid reducing processes needed to improve the efficiency of hydrothermal alteration, thus increasing chemical rock leaching and concurrent modification of fluid composition. The thermal Na–Cl water discharged at Ferraria is, in fact, strongly enriched with metals like Sr and Mn; these elements form stable aqueous oxoanions and/or metal-chloride complexes. Conversely, elements such as Al, Fe and As exhibit comparatively low concentrations because they are removed from the solution as critical conditions for the development of several neo-formed mineral phases are gradually attained. Thermodynamic equilibrium calculations, carried out by means of the PHREEQC software code (Parkhurst and Appelo 1999; Version 2), are consistent with this interpretation and show that the thermal fluid can precipitate Fe^{3+}-(hydr-)oxides, kaolinite and non-crystalline silica. Complementary numeric simulations, considering the 50% mix of seawater with a pristine fluid to

obtain the composition of the Ferraria thermal water, reveal that the silica leached from hydrothermally modified rocks and transferred to the thermal fluid before seawater mixing can reach 317 mg/L; the SiO_2 geothermometer can not be used in these circumstances to estimate the reservoir temperature, because silica should result predominantly from the rock acid leaching, as indicated by pH values and total dissolved CO_2(g).

The rock sections intersected by AC1 and AC2 wells show evidence for fracture-controlled hydrothermal circulation. The interconnected fracture-network is particularly important between 18- and 19-m depth, suggesting that this level may correspond to the most external flow-out zone, especially during major depressurising events. The available data indicate also that volcanic rocks intersected from 21 to $\approx$24 m depth, preserve features due to (pervasive) interaction with thermal fluids, comprising neo-formed mineral assemblages. Fracture planes and pores are covered and fully/partly filled up with polyphase botryoidal aggregates that locally show rhythmic growing and are mostly composed of goethite + ferrihydrite, the latter displaying variable adsorbed contents of Si, P and As. These are very similar to Fe–Si precipitates (regularly containing adsorbed Ca, P and As) commonly reported in varied hydrothermal systems, of high and low temperature, mostly development under submarine volcanic settings (e.g. Iizasa 1993). In fact, the easy way to promote the formation of Fe^{3+}-(hydr-)oxides in those settings is through changing of redox conditions achieved when the thermal fluid mixes with colder and oxygenated seawater; under these circumstances, seawater phosphate and other oxyanion species (such as As) may co-precipitate (e.g. Berner 1973, Feely et al. 1990, 1991).

Redox reactions determine most of the As behaviour in solution; but these tend to proceed as a response to changes in redox equilibrium and redox potential controlled by reactions involving major elements (such as O, C, N, S and Fe). The oxidation reaction of As(III) by dissolved O_2 is rather slow; Johnson and Pilson (1972) report half-lives for the As(III) oxygenation in seawater ranging from several months to a year. However, according to Feely et al. (1994), the formation of Fe^{3+}-(hydr-)oxides enriched with Si, P and As may occur within few minutes to hours after seawater mixing with hydrothermal fluids near seafloor conditions because of fast Fe^{2+}-oxidation rate and low Fe^{3+} solubility in seawater (Rudnicki and Elderfield 1993). For the Ferraria thermal water, the dissolved As and Fe co-vary and is consistent with the observed neo-formed phases in the heterogeneously altered basalt of the lava delta; this co-variation seems to be independent of the seawater mixing degree and does not influence either the electric conductivity, or the concentration of dissolved silica or conservative elements (as Cl). Consequently, the high As contents occasionally recorded by the thermal water pumped at AC3 may be caused by: (1) pH and redox variations in the pristine fluid due to an increment of volcanic gases (namely, CO_2 and H_2S); and/or (2) fluid pressure fluctuations in the fractured aquifer; and/or (3) sudden oscillation in flow-velocity. It should be noted that the latter two mechanisms could be triggered by the well pumping operation.

The P, also detected in the neo-formed phases, is presumably taken from the seawater circulating through the basaltic lava delta; phosphate shares many chemical characteristics with arsenate and, in oxidised and biologically productive surface marine waters, its depletion is mirrored by arsenate reduction (Smedley and Kinniburgh 2002). The most common process of phosphate removal from seawater is by Fe^{3+}-(hydr-)oxide adsorption, and this requires relatively cool and oxidising seawater.

Acknowledgments This work was funded by INOVA Institute through a contract with Faculdade de Ciências, Universidade de Lisboa, at the aim of the Project "Valorização de Águas Termais dos Açores", funded by the EU-PRODESA Programme and the Azores Government (Secretaria Regional da Economia). INOGAZ project (PTDC/CTE-GIN/68851/2006) released δ^2H and δ^{18}O isotopic data. The authors acknowledge Eng. Diamantino Oliveira, Head of the Geological Resources Division of Secretaria Regional da Economia, for his cooperation on AC1 and AC2 drill-hole logging, as well as the suggestions of an anonymous reviewer which contributed to clarify the ideas presented in this paper.

References

Arnórsson S (1991) Geochemistry and geothermal resources in iceland. Science Inst. University of Iceland, Reykjavik, p 68

Berner RA (1973) Phosphate removal from sea water by adsorption on volcanogenic ferric oxides. Earth Planet Sci Lett 18:77–86

Carvalho MR (1999) Hidrogeologia do maciço Vulcânico de Água de Pau/Fogo, S. Miguel, Açores. PhD dissertation, Universidade de Lisboa, Lisboa, 445 p

Coutinho R (1990) Estudo hidrogeológico do Maciço das Sete Cidades. Mcs dissertation, Universidade de Lisboa, Lisboa, 134 p

Coutinho R, Carreira PM, Almeida C, Monge Soares AM, Vieira MCR, Carvalho MR, Cruz JV (1996) Estudo isotópico dos sistemas aquíferos do Maciço das Sete Cidades, S. Miguel—Resultados preliminares. Recursos Hídricos 17:25–32

Cruz JV, Coutinho R, Carvalho MR, Óskarsson N, Gíslason S (1999) Chemistry of waters from the Furnas Volcano, São Miguel, Azores: Fluxes of volcanic carbon dioxide and leached material. J Volcanol Geotherm Res 92:151–167

Feely RA, Massoth GJ, Baker ET, Cowen JP, Lamb MF, Krogslund KA (1990) The effect of hydrothermal processes on mid-water phosphorus distribution in the northeast Pacific. Earth Planet Sci Lett 96:305–318

Feely RA, Trefry JH, Massoth GJ, Metz S (1991) A comparison of the scavenging of phosphorus and arsenic from seawater by hydrothermal iron oxyhydroxides in the Altantic and Pacific oceans. Deep Sea Res 38:617–623

Feely RA, Massoth GJ, Trefry JH, Baker ET, Paulson AJ, Lebon GT (1994) Composition and sedimentation of hydrothermal plume particles from North Cleft segment, Juan de Fuca Ridge. J Geophys Res 99:4985–5006

Forjaz VH (1994) Geologia económica e aplicada da ilha de S. Miguel (Açores): recursos vulcanogeotérmicos. PhD Disstatio. Universidade Açores, Ponta Delgada, Açores, 599 p

Freire, P (2006) Águas minerais da Ilha de S. Miguel (Açores): caracterização hidrogeológica e implicações para a monitorização vulcanológica. Mcs Dissertation, Universidade dos Açores, Ponta Delgada, Açores, 272 p

Iizasa K (1993) Petrographic investigations of seafloor sediments from the Kita-Bayonnaise submarine caldera. Schichito-Iwojima Ridge. Izu-Ogasawara Arc, northwestern. Pac Mar Geol 112:271–290

Johnson DL, Pilson EQ (1972) Spectrophotometric determination of arsenite, arsenate, and phosphate in natural waters. Anal Chim Acta 58:289–299

Moore RB (1991) Geologic Map of São Miguel, Azores. Escala 1:50 000. In: US Geological Survey (ed) Miscellaneous Investigation Series. US Department of the Interior

Nunes, JC (2004) Geologia. In: Forjaz, VH (ed) Atlas Básico dos Açores. Observatório Vulcanológico e Geotérmico dos Açores. Ponta Delgada, pp 60–62

Nunes JC, França Z, Forjaz VH, Macedo R, Lima EA (2004) Poligenetic volcanoes of Azores archipelago (Portugal): size, nature, eruptive styles and related volcanic hazard. Poster—32nd International Geological Congress—Abstracts (Part 1). Agosto. Firenze. Itália, 336 p

Parkhurst DL, Appelo CAJ (1999) User's guide to PHREEQC (version 2) A computer program for speciation, batch-reaction, one-dimensional transport, and inverse geochemical calculations. Water-Resources Investigations Report 99-4259. US Geological Survey, Denver

Rudnicki MD, Elderfield H (1993) A chemical model of the buoyant and neutrally buoyant plume above the TAG vent field, 26 degrees N, Mid-Atlantic Ridge. Geochim Cosmochim Acta 57:2939–2957

Smedley PL, Kinniburgh DG (2002) A review of the source, behaviour and distribution of arsenic in natural waters. Appl Geochem 17:517–568